Slip flow boundary conditions in discontinuous Galerkin discretizations of the Euler equations of gas dynamics

J.J.W. van der Vegt and H. van der Ven

Slip flow boundary conditions in discontinuous Galerkin discretizations of the Euler equations of gas dynamics

J.J.W. van der Vegt and H. van der Ven

This report is based on a presentation held at the fifth World Congress on Computational Mechanics, Vienna - Austria on 7-12 July 2002.

Summary

Discontinuous Galerkin discretizations of the slip flow boundary condition at curved walls in inviscid gas dynamics are not very accurate when linear basis functions are combined with elements with straight edges at the boundary. This is particularly true when the boundary integrals are computed with a Gauss quadrature rule, but also occurs when the more accurate Taylor quadrature rule is used. The error at the solid surface results in a boundary layer which can significantly pollute the numerical solution. In this paper sources of these problems are analyzed and demonstrated for the subsonic flow about a circular cylinder. It is shown that the use of the recently developed Taylor quadrature rule for the flux integrals in combination with superparametric elements results in more than a factor three reduction in total pressure loss at the wall in comparison with isoparametric elements and Gauss quadrature. The effects of boundary curvature can also be removed using mesh adaptation. Local mesh refinement of linear isoparametric elements is very effective in reducing the error at slip flow boundaries and provides a good alternative to the use of superparametric elements. This is possible because it is demonstrated that it is not necessary to use a higher-order boundary representation.

Contents

7 Figures

(26 pages in total)

1 Introduction

Discontinuous Galerkin finite element methods (DGFEM) provide a new numerical discretization technique for the Euler equations of gas dynamics. The DGFEM is a combination of an upwind finite volume scheme and a finite element method, with as key feature the use of local polynomial basis functions to represent the test and trial functions. These basis functions are only weakly coupled to neighboring elements, which make discontinuous Galerkin methods ideally suited for mesh adaptation using local mesh refinement. The discontinuous Galerkin finite element method for hyperbolic conservation laws has been pioneered by Cockburn and Shu (for a general survey see (Ref. 4, 5)). Discontinuous Galerkin methods for the Euler equations with local mesh refinement are described in Baumann and Oden (Ref. 3) and Van der Vegt and Van der Ven (Ref. 8). Recently, the DGFEM has been extended by Van der Vegt and Van der Ven (Ref. 9) to basis functions which are discontinuous in both space and time. This so-called space-time DGFEM is well suited for problems with time-dependent boundaries, which require moving and deforming meshes. Aerodynamic applications, such as oscillating and deforming wings, can be found in (Ref. 9, 10).

In most of the flow domain DG finite element methods result in an accurate numerical discretization, but at solid surfaces, where a slip flow boundary condition must be applied in inviscid gas dynamics, DGFEM suffers from a significant loss in accuracy. This was first demonstrated by Bassi and Rebay (Ref. 1) for the smooth subsonic flow about a circular cylinder, where in the near wall region and wake of the cylinder a significant shear layer occurred, which is incorrect for inviscid flow. Bassi and Rebay showed that using linear polynomials for the test and trial functions in combination with quadratic superparametric elements significantly reduced this effect for triangular elements, but did not really give an explanation for this phenomenon. Recently, Van der Ven and Van der Vegt (Ref. 10) proposed a new so-called Taylor quadrature rule for the flux integrals in the space-time DGFEM to improve the numerical efficiency of the method. The Taylor quadrature rule results in a factor three improvement in performance, but it was noticed that it also results in a significantly reduced numerical shear layer for the flow about a circular cylinder, (Ref. 10). It seems that not only the choice of element type, namely isoparametric or superparametric, but also the flux quadrature rule and boundary discretization, directly affect the accuracy near a slip flow boundary.

The main objective of this paper is to investigate different techniques to improve the accuracy in the near wall region and wake of inviscid flows with a slip flow boundary condition. For subsonic flow the error caused by the slip flow boundary condition dominates the overall numerical error

and also generates unphysical vorticity and entropy near the wall. An improved discretization of the slip flow boundary condition is of great importance for many applications which require good accuracy in the near wall region, such as in aerodynamics. In this paper we will focus on the effects of the flux quadrature rule, element type, and the calculation of the wall pressure in combination with the HLLC flux proposed by Toro et al. (Ref. 6). Also, we will consider local mesh refinement based on the boundary curvature as an alternative technique to reduce the errors near a slip flow boundary.

Since the problems with the slip flow boundary conditions in discontinuous Galerkin methods occur both in two and three-dimensions, and are independent of the time integration technique, we limit the present discussion to simple two-dimensional steady flows. The results are, however, directly applicable to space-(time) DGFEM in three dimensions. In the remainder of this paper we first discuss the discontinuous Galerkin discretization for the Euler equations. Next, we discuss the evaluation of the element face and volume integrals using Gauss and Taylor quadrature rules, followed by the evaluation of the pressure at the slip wall. The effect of the different techniques is demonstrated with the subsonic flow about a circular cylinder.

2   Governing equations

The Euler equations for inviscid gas dynamics with initial and boundary conditions in a domain $\Omega \subset \mathbb{R}^2$ can be expressed as:

$$\frac{\partial}{\partial t}U(x,t) + \frac{\partial}{\partial x_j}F_j(U(x,t)) = 0, \qquad (x,t) \in \Omega \times (t_0, T], \qquad (1)$$

$$U(x,t) = \mathcal{B}(U, U_w), \qquad (x,t) \in \partial\Omega \times (t_0, T],$$

$$U(x,t_0) = U_0(x), \qquad x \in \bar{\Omega},$$

with $U : \bar{\Omega} \times [t_0, T] \to \mathbb{R}^4$ the vector of conserved quantities, $F_j : \mathbb{R}^4 \to \mathbb{R}^4$, $(j = 1, 2)$ the flux vectors, which are defined as:

$$U = \begin{pmatrix} \rho \\ \rho u_i \\ \rho E \end{pmatrix}, \qquad F_j = \begin{pmatrix} \rho u_j \\ \rho u_i u_j + p\delta_{ij} \\ u_j(\rho E + p) \end{pmatrix},$$

$\mathcal{B} : \mathbb{R}^4 \times \mathbb{R}^4 \to \mathbb{R}^4$ the boundary operator, with $U_w : \partial\Omega \times (t_0, T] \to \mathbb{R}^4$ the prescribed boundary data, $U_0 : \bar{\Omega} \to \mathbb{R}^4$ the data at the initial time $t = t_0$, and T represents the final time. In addition, ρ, $p, E : \bar{\Omega} \times [t_0, T] \to \mathbb{R}^+ \cup \{0\}$ denote the density, pressure and specific total energy, respectively, u_i, $(i = 1, 2)$ the components of the velocity vector $u : \bar{\Omega} \times [t_0, T] \to \mathbb{R}^2$ in the Cartesian coordinate direction x_i, and δ_{ij} the Kronecker delta symbol. The Euler equations are closed with an equation of state, for which we assume a calorically perfect gas: $p = (\gamma - 1)\rho(E - \frac{1}{2}u_i u_i)$, with γ the ratio of specific heats at constant pressure and constant volume. In this paper we use the summation convention on repeated indices.

3 Discontinuous Galerkin discretization

For the discontinuous Galerkin finite element discretization the domain Ω is approximated with a tessellation $\mathcal{T}_h$ of quadrilateral elements $K \in \mathcal{T}_h$, which are open domains and satisfy the condition $\cup_{K_j \in \mathcal{T}_h} \bar{K}_j := \bar{\Omega}_h \to \Omega$ as $h \to 0$, with h the radius of the smallest circle containing all elements $K \in \mathcal{T}_h$. In addition, the elements $K \in \mathcal{T}_h$ satisfy the condition $K_j \cap K_{j'} = \emptyset$ if $j \neq j'$. The elements $K \in \mathcal{T}_h$ are connected to a reference element $\hat{K} = [-1, 1]^2$, either through the isoparametric mapping G_K^1:

$$G_K^1 : \hat{K} \to K : \xi \mapsto x = \sum_{i=0}^{1} \sum_{j=0}^{1} x_{ij}(K)\hat{p}_i(\xi_1)\hat{p}_j(\xi_2), \tag{2}$$

with:

$$\hat{p}_0(\xi_i) = \tfrac{1}{2}(1 - \xi_i),$$
$$\hat{p}_1(\xi_i) = \tfrac{1}{2}(1 + \xi_i),$$

and $x_{ij}(K)$, $i, j \in \{0, 1\}$ the vertices of element K, or through the superparametric mapping G_K^2, which is defined as:

$$G_K^2 : \hat{K} \to K : \xi \mapsto x = \sum_{i=0}^{2} \sum_{j=0}^{2} x_{ij}(K)\hat{q}_i(\xi_1)\hat{q}_j(\xi_2), \tag{3}$$

with:

$$\hat{q}_0(\xi_i) = \tfrac{1}{2}\xi_i(\xi_i - 1),$$
$$\hat{q}_1(\xi_i) = 1 - \xi_i^2,$$
$$\hat{q}_2(\xi_i) = \tfrac{1}{2}\xi_i(\xi_i + 1),$$

and $x_{ij}(K)$, $i, j \in \{0, 1, 2\}$ the vertices, midpoints of the edges, and center of the element K.

The discontinuous Galerkin discretization uses basis functions in each element which are discontinuous across element faces. The DG basis functions are defined through the following steps:

- Define $P^1(\hat{K})$ as the space of polynomials $\hat{\phi} : \hat{K} \to \mathbb{R}$ of degree ≤ 1 on the reference element $\hat{K}$:

$$P^1(\hat{K}) := \text{span}\{\hat{\phi}_j \mid j = 0, 1, 2\}.$$

- Define $P_m^1(K)$, $(m = 1, 2)$, as the space of functions $\phi : K \to \mathbb{R}$ associated to functions in $P^1(\hat{K})$ through the mapping G_K^m, (2)-(3):

$$P_m^1(K) := \text{span}\{\phi_j = \hat{\phi}_j \circ (G_K^m)^{-1} \mid j = 0, 1, 2\}.$$

- Define the space of functions $\bar{P}_m^1(K) := \text{span}\{\psi_j \mid j = 0, 1, 2\}$, with the basis functions $\psi_j : K \to \mathbb{R}$ defined as:

$$\psi_0(x) = 1,$$

$$\psi_j(x) = \phi_j(x) - \frac{1}{|K|} \int_K \phi_j(x) dK, \qquad j = 1, 2.$$

- Define the function space $V_{m,h}^1(K)$ as:

$$V_{m,h}^1(K) := \{(p_1, \cdots, p_4)^T : K \to \mathbb{R}^4 \mid p_i \in \bar{P}_m^1(K)\},$$

then the vector of conservative variables $U_{|K}$ can be approximated as $U_h : K \times [t_0, T] \to \mathbb{R}^4$ as:

$$U_h(x,t) := \mathcal{P}(U_{|K}) = \sum_{j=0}^{2} \hat{U}_{m,K}(t)\psi_j(x), \qquad \text{for } x \in K, \tag{4}$$

with $\mathcal{P}$ the projection operator to the finite-dimensional space $V_{m,h}^1(K)$ and $\hat{U}_{m,K} \in \left(C^1([t_0, T])\right)^4$. The weak form in each element $K \in \mathcal{T}_h$ for the Euler equations of gas dynamics can now be defined as:

Find a $U_h \in V_{m,h}^1(K)$, such that $U_h(x, 0) = \mathcal{P}(U_0(x))$, and for all $W_h \in V_{m,h}^1(K)$ the following relation is satisfied:

$$\frac{d}{dt} \int_K W_h \cdot U_h dK = -\int_{\partial K} W_h \cdot H(U_L, U_R) dS + \int_K \frac{\partial W_h}{\partial x_j} F_j(U_h) dK. \tag{5}$$

The weak formulation is obtained by multiplying the Euler equations (1) in each element $K \in \mathcal{T}_h$ with the test functions $W_h \in V_{m,h}^1(K)$, integration by parts over the element K, and finally a summation over all elements in $\mathcal{T}_h$. Weak continuity at the element faces ∂K is ensured by introducing the numerical flux $H : \mathbb{R}^4 \times \mathbb{R}^4 \to \mathbb{R}^4$. This is accomplished by considering the traces U_L and U_R of U_h in the boundary integrals of the elements K_j and $K_{j'}$, which satisfy the condition $\bar{K}_j \cap \bar{K}_{j'} \subset \partial K$, as the initial data of a Riemann problem. For the present subsonic flow calculations no stabilization operator was necessary. More details, including the derivation of the weak formulation for the space-(time) discontinuous Galerkin finite element method, can be found in Van der Vegt and Van der Ven (Ref. 9).

The discontinuous Galerkin finite element discretization is now obtained if we introduce the polynomial representations for the test and trial functions W_h and U_h, given by (4), into the weak formulation (5) and conduct the element integrations:

$$\frac{d\hat{U}_m}{dt} \int_K \psi_i \psi_m dK = -\int_{\partial K} \psi_i H_i(U_L, U_R) dS + \int_K \frac{\partial \psi_i}{\partial x_j} F_j(U_h) dK, \qquad i = 0, 1, 2. \tag{6}$$

The resulting equations for the polynomial coefficients are solved using a Runge-Kutta time integration method in combination with a multigrid convergence acceleration technique. In this paper we only consider steady state solutions, but for implicit time-accurate calculations a pseudo-time integration technique is used to solve the non-linear equations for the expansion coefficients. For more details see (Ref. 9).

4 Numerical flux function

The introduction of the numerical flux introduces upwinding into the finite element discretization and any monotone and consistent (approximate) Riemann solver for the Euler equations of gas dynamics can be used as numerical flux. In the present research we use the HLLC flux proposed by Toro et al. (Ref. 2, 6), see also Toro (Ref. 7). This is motivated by the fact that this approximate Riemann solver combines good accuracy with a low computational cost. In addition, the HLLC flux combines well with the Taylor quadrature rule for the fluxes to be discussed in the next section. The HLLC flux in a form suitable for the Taylor quadrature integration can be summarized as:

$$
\begin{aligned}
H(U_L, U_R) = & c_L \hat{F}(U_L) + c_R \hat{F}(U_R) - (c_L + c_R - 1)p^* v_p + \\
& \tfrac{1}{2}\big(|S_L| - S_L \frac{|S_L| - |S_M|}{S_L - S_M}\big)U_L - \tfrac{1}{2}\big(|S_R| - S_R \frac{|S_R| - |S_M|}{S_R - S_M}\big)U_R,
\end{aligned}
$$

with $\hat{F} = n_j F_j : \partial K \to \mathbb{R}^4$ the normal flux vector and $n : \partial K \to \mathbb{R}^2$ the unit outward normal vector at ∂K. The coefficients $c_{L,R} \in \mathbb{R}$ are defined as:

$$
c_L = \tfrac{1}{2}\Big(1 + \frac{|S_L| - |S_M|}{S_L - S_M}\Big), \qquad c_R = \tfrac{1}{2}\Big(1 - \frac{|S_R| - |S_M|}{S_R - S_M}\Big).
$$

The intermediate pressure $p^* \in \mathbb{R}^+$ is equal to:

$$
p^* = \rho_L(S_L - \hat{u}_L)(S_M - \hat{u}_L) + p_L,
$$

with $\hat{u} = n \cdot u$ the normal velocity, and the vector $v_p \in \mathbb{R}^4$ is defined as $v_p = (0, n, S_M)^T$. The wave speeds S_L and S_R are defined as:

$$
S_L = \min(\hat{u}_L - a_L, \hat{u}_R - a_R), \qquad S_R = \max(\hat{u}_L + a_L, \hat{u}_R + a_R)
$$

with $a = \sqrt{\gamma p / \rho}$ the speed of sound. The contact wave speed S_M is equal to:

$$
S_M = \frac{\rho_R \hat{u}_R(S_R - \hat{u}_R) - \rho_L \hat{u}_L(S_L - \hat{u}_L) + p_L - p_R}{\rho_R(S_R - \hat{u}_R) - \rho_L(S_L - \hat{u}_L)}.
$$

The suffices L and R refer to the internal and external flow states at the element boundary, respectively.

5 Flux quadrature

An important aspect in the discontinuous Galerkin discretization is the calculation of the flux integrals in (6). This influences both the accuracy and efficiency of the method. In general these integrals are computed with product Gauss quadrature rules, with two quadrature points in each coordinate direction. This ensures a sufficiently accurate evaluation of the integrals, but also requires the evaluation of the numerical flux function at each quadrature point. Especially in three-dimensions and for the space-time discontinuous Galerkin finite element method this quickly becomes computationally very expensive. In order to alleviate this problem the Taylor quadrature rule was proposed and analyzed by Van der Ven and Van der Vegt (Ref. 10). The Taylor quadrature rule has as main benefit that it requires only one flux evaluation per element face or volume integral. Apart from being computationally more efficient it was also observed in (Ref. 10) that this integration technique results in a smaller error at solid walls with a slip flow boundary condition. In this and the remaining sections we will further investigate this and propose further improvements to the numerical discretization of slip flow boundary conditions.

The first step in the evaluation of the integrals in (6) is to transform the integrals on the righthand side into integrals over the reference element:

$$\int_{\partial K} \psi_i(x) H_i(U_L, U_R) dS = \sum_{k=1}^{4} \int_{\hat{e}_k} \hat{\psi}_i(\xi) H_i(U_L, U_R) \left| \frac{\partial G_K^m}{\partial \xi_l} \right| d\xi_l,$$

$$\int_K \frac{\partial \psi_i}{\partial x_j} F_j(U_h) dK = \int_{\hat{K}} \frac{\partial \hat{\psi}_i}{\partial \xi_j} F_j(U_h) \left| J_{G_K^m} \right| d\xi_1 d\xi_2,$$

with $l = 1$ if $k = 1, 2$ and $l = 2$ if $k = 3, 4$; $\hat{\psi}_i(\xi) = \psi_i(G_K^m(x))$ and $\hat{e}_k \subset \partial \hat{K}$ one of the four faces of the reference element $\hat{K}$.

The Gauss quadrature rule now approximates the surface flux integrals as:

$$\int_{\hat{e}_k} \hat{\psi}_i(\xi) H_i(U_L, U_R) \left| \frac{\partial G_K^m}{\partial \xi_l} \right| d\xi_l \cong \sum_{n=1}^{N_{Gauss}} w_n \hat{\psi}_i(\xi_n) H_i(U_L(\xi_n), U_R(\xi_n^*)) \left| \frac{\partial G_K^m(\xi_n)}{\partial \xi_l} \right|,$$

with $w_n \in \mathbb{R}^+$ the quadrature weights, $N_{Gauss} \in \mathbb{N}$ the number of Gauss quadrature points, and $\xi_n, \xi_n^* \in (-1, 1)$ the quadrature points at both sides of the element face. Note, ξ_n and ξ_n^* are not necessarily the same since the elements at both sides of the face might have a local coordinate system with a different orientation. The evaluation of the volume integrals is completely analogous.

For the Taylor quadrature rule we split the numerical flux function $H(U_L, U_R)$ into two parts:

$$H(U_L, U_R) = \tfrac{1}{2}(n_j F_j(U_L) + n_j F_j(U_R)) - D(U_L, U_R),$$

where $D(U_L, U_R)$ represents the numerical dissipation of the HLLC scheme. The integrals are now evaluated using a Taylor series expansion of the flux at the element face center:

$$\int_{\hat{e}_k} \hat{\psi}_i(\xi) F_j(U) dS_j \cong F_j(U(\bar{\xi})) \int_{\hat{e}_k} \hat{\psi}_i(\xi) dS_j + \frac{\partial F_j(U)}{\partial U_k} \frac{\partial U_k(\bar{\xi})}{\partial \xi_p} \int_{\hat{e}_k} \xi_p \hat{\psi}_i(\xi) dS_j, \qquad (7)$$

with $dS : \hat{e}_k \rightarrow \mathbb{R}^2$ a vector measure which is defined as: $dS = n \left| \frac{\partial G_K^m}{\partial \xi_l} \right| d\xi_l$, and $U = U_L$ or U_R. The integrals on the righthand side of (7) can be evaluated analytically and result in simple expressions, see (Ref. 10). The derivatives of the flow state U_h in (7) can be computed directly from the polynomial representation of U_h given by (4), and are equal to: $\frac{\partial U_h}{\partial \xi_l} = \hat{U}_l$. The discontinuous Galerkin discretization therefore automatically provides the necessary data for the Taylor quadrature. The integrals containing the dissipative part of the HLLC flux are evaluated analogously. It is, however, not necessary to compute exact derivatives of $\frac{\partial D}{\partial \xi_l}$ to preserve accuracy and stability and we assume that S_L and S_R are constant during the integration process, see (Ref. 10) for more details. The evaluation of the volume integrals is analogous to the flux integrals and not further discussed.

6 Slip flow boundary

At a slip flow boundary we impose the boundary condition:

$$u \cdot n = 0, \qquad \text{at } \partial\Omega_s \subseteq \partial\Omega.$$

This implies that the pressure is the only non-zero contribution in the flux at the domain boundary $\partial\Omega_s$. The zero normal velocity at $\partial\Omega_s$ can be imposed using ghostcells at the wall, where the velocity is equal to:

$$\rho_R u_R = \rho_L u_L - 2\rho_L (u_L \cdot n)n,$$

and is used in the Gauss quadrature of the flux at the domain boundary faces. This has as main benefit that the same HLLC flux function can be used both for faces in the interior and at the domain boundary. The straightforward implementation of the Taylor flux quadrature requires, however, derivatives $\frac{\partial U_R}{\partial U_L}$, since $U_R = U_R(U_L)$, and this results in a flux at the wall which does not only depend on the pressure, as is required by the exact boundary condition. In order to remove this inconsistency we use at the boundary faces the pressure which is obtained from the exact solution of the Riemann problem for a reflective wall. This solution is relatively simple and consists either of two rarefaction or two shock waves, see Toro (Ref. 7), and can be summarized as:

If $u_L \leq 0$ (rarefaction wave):

$$p^* = p_L \left[1 + \frac{(\gamma - 1)u_L}{2a_L} \right]^{\frac{2\gamma}{\gamma-1}}, \qquad \text{with } a_L = \sqrt{\frac{\gamma p_L}{\rho_L}}.$$

If $u_L > 0$ (shock wave):

$$p^* = p_L + \frac{u_L}{2A_L} \left(u_L + \sqrt{u_L^2 + 4A_L(p_L + B_L)} \right),$$

with:

$$A_L = \frac{2}{(\gamma + 1)\rho_L}, \qquad B_L = \frac{(\gamma - 1)}{(\gamma + 1)} p_L.$$

Here the suffix L refers to the internal flow state at the wall at the initial time of the Riemann problem. The pressure p^* in the Riemann problem ensures that slip flow boundary condition $u^* \cdot n = 0$ is satisfied, with u^* the velocity at the wall in the exact Riemann problem. The evaluation of the boundary flux integral $\int_{\hat{e}_K} p^* n |\partial G_K^m / \partial \xi_l| d\xi_l$ with the Taylor quadrature rule is now straightforward and significantly improves the accuracy in the near wall region when it is combined with a sufficiently accurate representation of the boundary geometry.

The integration of the boundary flux $F(U_w) = (0, p^*n, 0)$ with the Gauss quadrature rule does not give any noticeable difference in comparison with the use of the pressure in the star region obtained from the HLLC flux using ghostcells.

7 Effect of wall curvature on the accuracy of the discontinuous Galerkin discretization

The accuracy in the near wall region of the discretization of the slip flow boundary condition does not only depend on the evaluation of the boundary integrals, but also on the representation of the surface geometry. This was noticed by Bassi and Rebay (Ref. 1), where they showed that the use of superparametric elements improved the accuracy in the near wall region. In this section we will analyze the effect of the boundary representation on the accuracy of the domain boundary integrals when they are evaluated with the Taylor quadrature rule. If we expand the flux function $\tilde{F}_j(\xi) = F_j(U(G_K^m(\xi)))$ and the mapping $G_K^m(\xi)$ in a Taylor series terms of ξ around the point $\bar{\xi}$, with $\xi = \xi_1$ or ξ_2 depending on the index k of $\hat{e}_k$, then we obtain:

$$\int_{\hat{e}_k} \hat{\psi}_i(\xi) F_j(U) dS_j \cong \big(\tilde{F}_j(\bar{\xi}) S_j(\bar{\xi})\big) \int_{\hat{e}_k} \hat{\psi}_i(\xi) d\xi + \Big(\frac{\partial \tilde{F}_j(\bar{\xi})}{\partial \xi} S_j(\bar{\xi}) + \tilde{F}_j(\bar{\xi}) \frac{\partial S_j(\bar{\xi})}{\partial \xi}\Big) \int_{\hat{e}_k} \xi \hat{\psi}_i(\xi) d\xi,$$

with $S_j = n_j |\frac{\partial G_K^m}{\partial \xi}|$. Introduce the arclength $s(\xi) := \int_{-1}^{\xi} |\frac{\partial G_K^m}{\partial \xi'}| d\xi'$, and use the relations:

$$S(\xi) = n^p(s) \frac{ds}{d\xi},$$

$$\frac{dS(\xi)}{d\xi} = -\kappa(s) t(s) \left(\frac{ds}{d\xi}\right)^2 + n^p(s) \frac{d^2 s}{d\xi^2},$$

with $t : [-1, 1] \to \mathbb{R}^2$ the tangential vector at the boundary curve $x = x(\xi) = \tilde{x}(s) \subset \partial K$, which is defined as $t(s) = \frac{d\tilde{x}(s)}{ds}$, $\kappa : [-1, 1] \to \mathbb{R}^+ \cup \{0\}$ the boundary curvature $k(s) = |\frac{d^2 \tilde{x}}{ds^2}|$, and $n^p : [-1, 1] \to \mathbb{R}^2$ the principal normal vector $n^p(s) = \frac{1}{\kappa} \frac{d^2 \tilde{x}}{ds^2}$. The boundary flux integrals can now be expressed as:

$$\int_{\hat{e}_k} \hat{\psi}_i(\xi) F_j(U) dS_j \cong \big(\tilde{F}_j(\bar{\xi}) n_j^p(\bar{s})\big) \frac{ds(\bar{\xi})}{d\xi} \int_{\hat{e}_k} \hat{\psi}_i(\xi) d\xi + \Big(\frac{\partial \tilde{F}_j(\bar{\xi})}{\partial \xi} n_j^p(\bar{s}) \frac{ds(\bar{\xi})}{d\xi} +$$
$$\tilde{F}_j(\bar{\xi})\big(-\kappa(\bar{s}) t_j(\bar{s}) \left(\frac{ds(\bar{\xi})}{d\xi}\right)^2 + n_j^p(\bar{s}) \frac{d^2 s(\bar{\xi})}{d\xi^2}\big)\Big) \int_{\hat{e}_k} \xi \hat{\psi}_i(\xi) d\xi,$$

with $\bar{s} = s(\bar{\xi})$. This expression shows that for a consistent boundary treatment in a discontinuous Galerkin discretization it is necessary to take the boundary curvature also into account. If we use linear elements, generated with the mapping G_K^1, then the contribution $-\kappa(s) t(s) (\frac{ds}{d\xi})^2 + n^p(s) \frac{d^2 s}{d\xi^2}$ is zero, but depending on the curvature κ this contribution can be large and non-negligible. For superparametric elements, generated with the mapping G_K^2, it is possible to take the boundary curvature into account and it can be expected that this results in a more accurate discretization at the boundary. This confirms the result from Bassi and Rebay (Ref. 1), which showed that using superparametric elements significantly improved the accuracy near the boundary. The use of su-
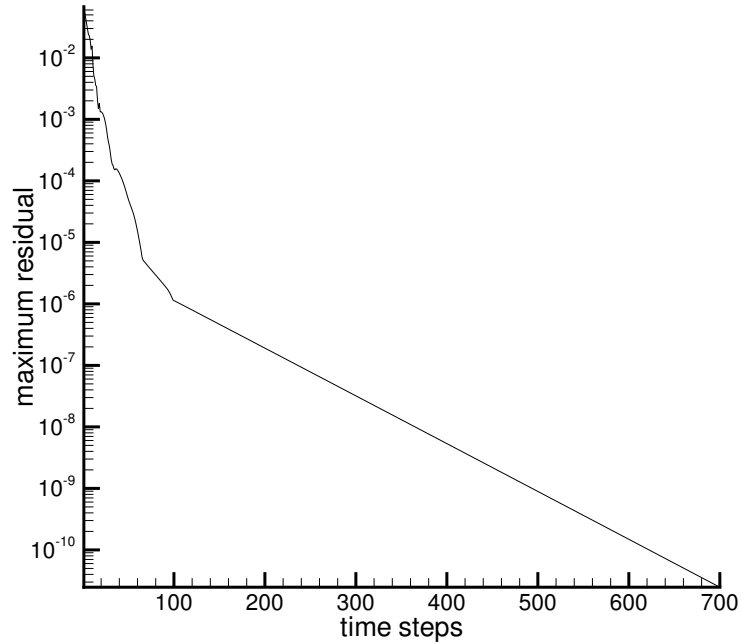
*Fig. 1   Maximum residual for all equations of the expansion coefficients $\hat{U}_m(K)$, $(m = 0, 1, 2)$
for the flow about a circular cylinder at $M_\infty = 0.38$ using a Gauss flux quadrature rule
and linear isoparametric elements (32×48 mesh).*

perparametric elements requires, however, significant modifications to a general three-dimensional DGFEM code. An alternative is provided by using linear elements, generated with the mapping G_K^1, and use local mesh refinement based on the local boundary curvature. This can effectively reduce the contribution $-\kappa(s)t(s)\left(\frac{ds}{d\xi}\right)^2 + n^p(s)\frac{d^2s}{d\xi^2}$ to such a small value that the element curvature becomes negligible. In the next section we will investigate both the use of superparametric elements and local mesh refinement.
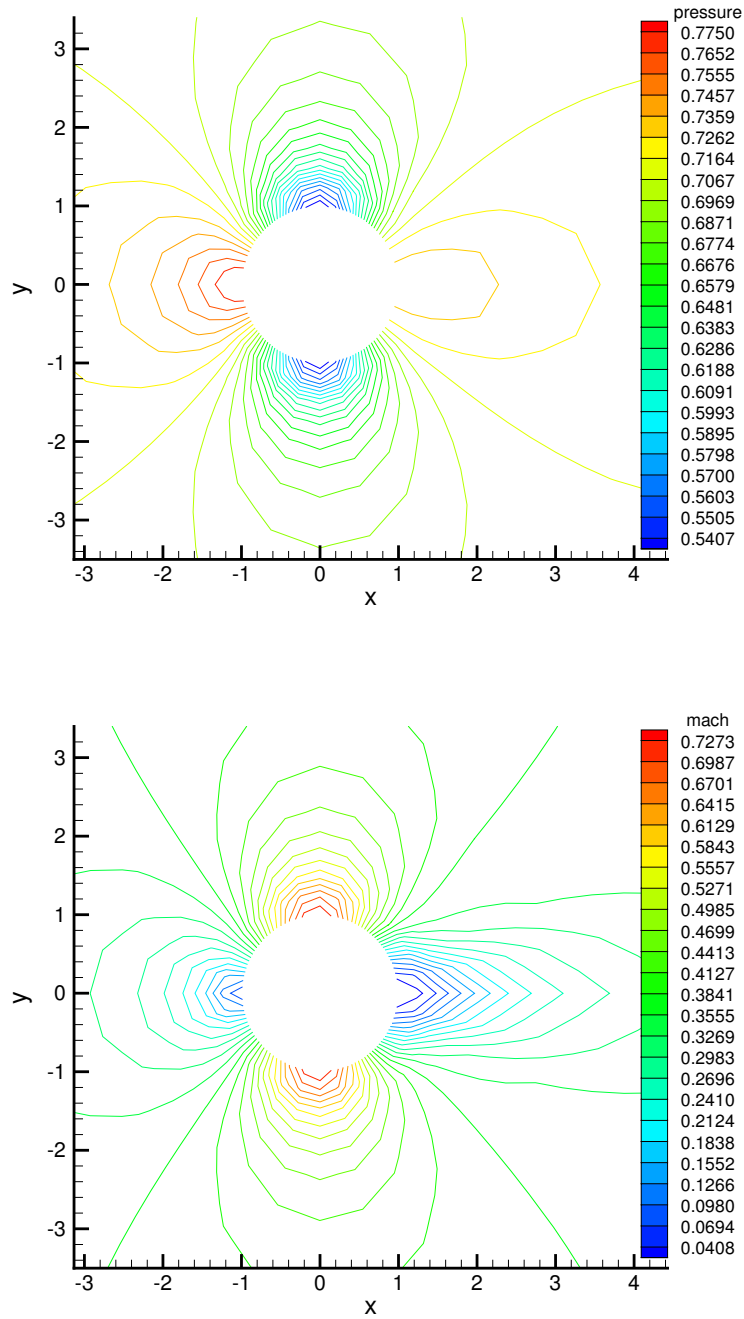
Fig. 2   Pressure field and Mach number contours for the flow about a circular cylinder at $M_\infty = 0.38$ using a Gauss flux quadrature rule and linear isoparametric elements (32×48 mesh).

8 Results

In order to investigate the effect of the different numerical discretizations for a slip flow boundary we consider the flow about a circular cylinder with a radius of one at the Mach number $M_\infty = 0.38$. This is the same problem as considered by Bassi and Rebay (Ref. 1) and is a good test case since it is very sensitive to the correct treatment of the slip flow boundary condition. If $M_\infty \to 0$ the solution is equal to the classical potential flow around a circular cylinder. The Mach number 0.38 is chosen in this study in order to avoid the well known difficulties of computing low Mach number flows which are not relevant for the present study. At the inflow we use the conditions $\rho_R u_R = \rho_\infty u_\infty$, $h_R = h_\infty$ and $p_R = p_L$, with h the specific total enthalpy, $h = E + p/\rho$. At the outflow boundary we use the conditions $\rho_R u_R = \rho_L u_L$, $h_R = h_L$ and $p_R = p_\infty$. The suffix ∞ refers to the free stream value and L to the internal flow state. For all calculations the residual in each of the equations for the coefficients $\hat{U}_m(K)$, $(m = 0, 1, 2)$, was reduced to 10^{-11} using a multigrid convergence acceleration technique. Figure 1 shows the result for linear isoparametric elements and Gauss flux quadrature. It should be noted that the results obtained by Bassi and Rebay (Ref. 1) for this case did not converge, even after more than 100.000 Runge-Kutta steps. In order to obtain converged solutions they had to use superparametric elements. As a measure for the accuracy of the different boundary discretizations we use the total pressure loss, which is defined as:

$$
p_{t-loss} = 1 - \frac{p}{p_\infty} \left(\frac{1 + \frac{1}{2}(\gamma - 1)M^2}{1 + \frac{1}{2}(\gamma - 1)M_\infty^2} \right)^{\frac{\gamma}{\gamma - 1}} .
$$

For subsonic inviscid flow the total pressure loss should be zero and is therefore a good indicator for the numerical accuracy. It is also an important quantity in aerodynamic computational fluid dynamics calculations, where it must be small otherwise the solution shows too much pollution through numerical dissipation and spurious vorticity generation.

For the baseline solution we use 32×48 linear isoparametric elements, generated with the mapping G_K^1. The boundary flux integrals are evaluated with a two-point Gauss quadrature rule with unit weights and quadrature points $\xi_n^* = \pm \frac{1}{\sqrt{3}}$, and a two-point product Gauss quadrature rule with the same weights and quadrature points for the volume integration. Figure 2 shows the pressure field and Mach number contours. For both quantities the contour lines are not very symmetric with respect to the axis $x = 0$. This is particularly true for the Mach number which clearly shows an artificial wake. The effect of the boundary condition becomes more pronounced when we look at the total pressure loss shown in Figures 3 and 4. The maximum value of the total pressure loss for linear isoparametric elements in combination with Gauss quadrature integration is 0.062. The use of quadratic superparametric elements in combination with Gauss quadrature reduces the
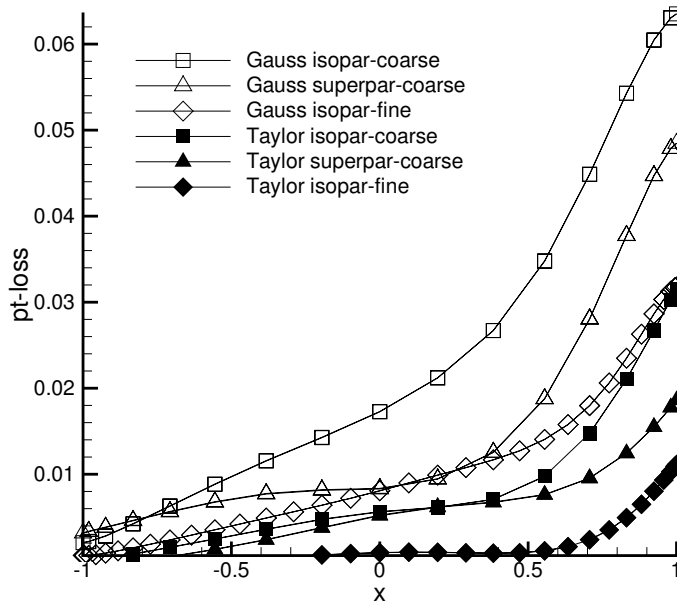
Fig. 3   Comparison of the total pressure loss at the wall for the flow around a circular cylinder
($M_\infty = 0.38$) using Gauss and Taylor flux quadrature rules for isoparametric elements
on a coarse (32×48 elements) and fine mesh (64×96 elements) and superparametric
elements on a coarse mesh (32×48 elements).

maximum value of the total pressure loss to 0.049, see Figure 3, which also shows the result on
the fine 64×96 mesh. The use of superparametric elements does reduce the total pressure loss for
a significant part of the boundary, which confirms the conclusion of Bassi and Rebay (Ref. 1) for
P1Q1 elements, but not sufficient near the rear stagnation line to remove the artificial wake. The
results on the 64×96 mesh in Figures 3 and 4 also show that the solution using Gauss quadrature
in combination with linear isoparametric elements improves on a fine mesh. This contradicts the
conclusion of Bassi and Rebay that a higher-order geometric approximation of curved boundaries
is mandatory in DGFEM. The difference can probably be attributed to the convergence problems
Bassi and Rebay experienced for this case, which resulted on a fine mesh in an unsteady flow.

For linear isoparametric elements in combination with the Taylor quadrature rule the total pressure
loss reduces to a maximum of 0.032, see Figures 3 and 4, which also show the result on the fine
64×96 mesh. A comparison of Taylor and Gauss quadrature techniques in Figure 3 shows that
the Taylor quadrature rule with linear isoparametric elements on the coarse 32×48 mesh has a
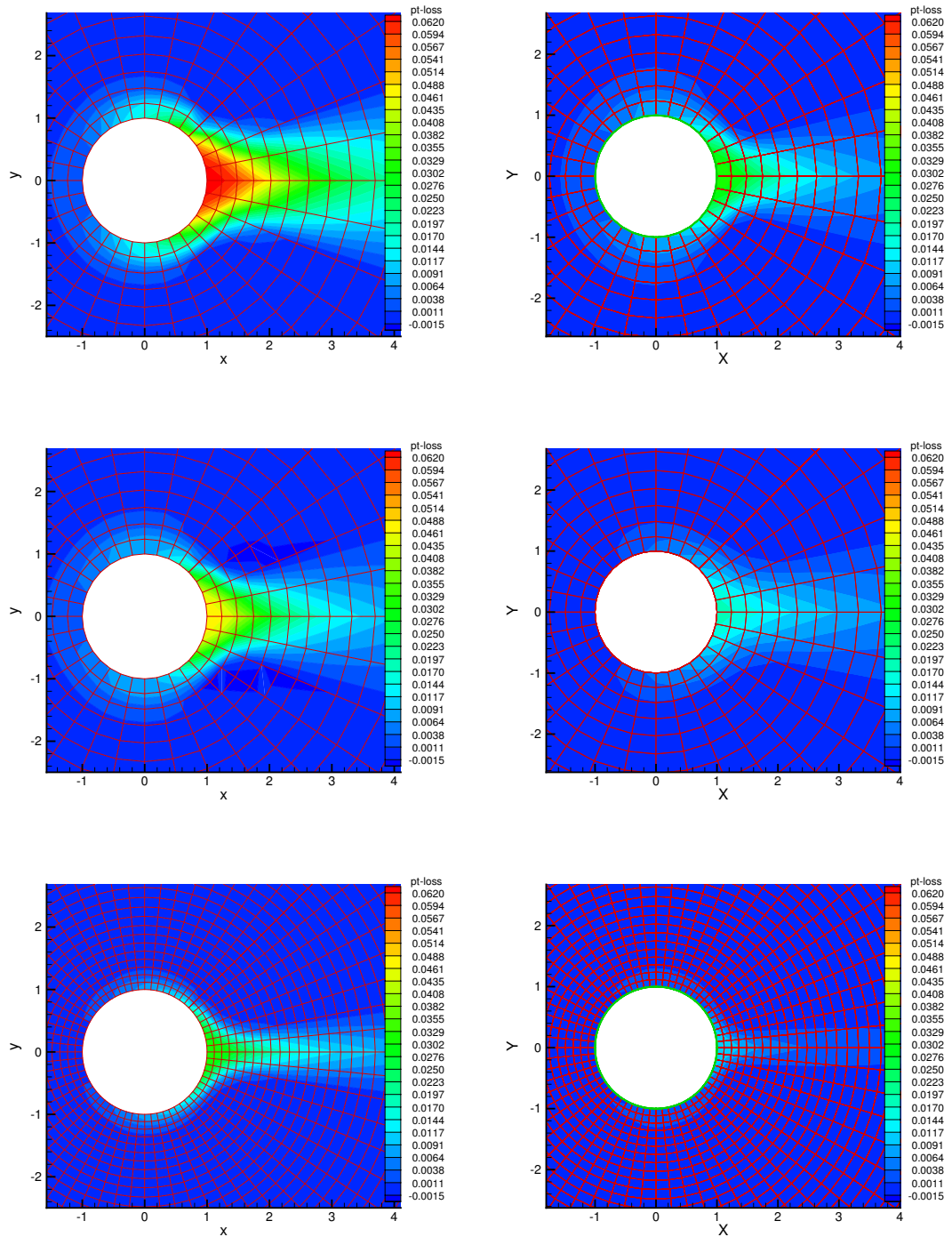comparable total pressure loss as linear isoparametric elements on the fine 64×96 mesh when

Fig. 4   Total pressure loss for flow around a circular cylinder at $M_\infty = 0.38$, using a Gauss quadrature rule (left) and Taylor quadrature rule (right). Top: linear isoparametric elements (32×48 mesh). Middle: quadratic superparametric elements (32×48 mesh). Bottom: linear isoparametric elements (64×96 mesh).
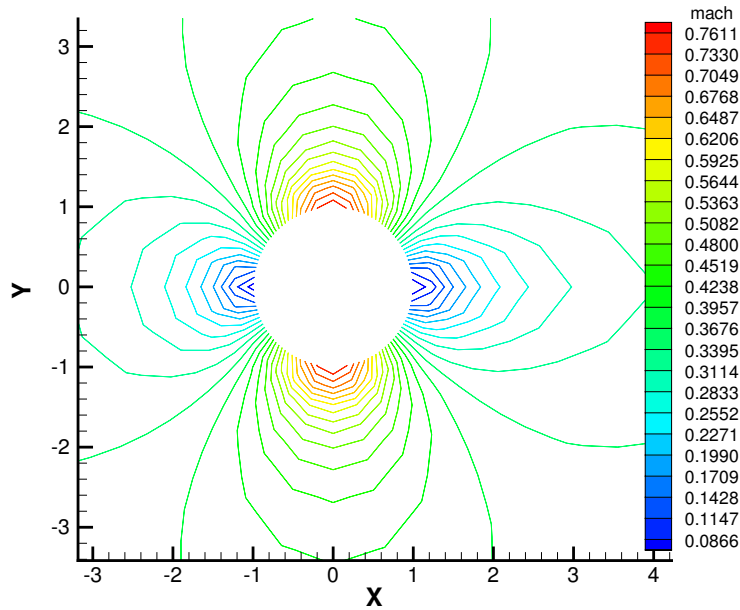
Fig. 5   Mach number contours for flow about a circular cylinder at $M_\infty = 0.38$ using Taylor quadrature and quadratic superparametric elements, wall pressure from Riemann problem (32×48 elements).

Gauss quadrature is used. This difference can be attributed to the fact that in the Gauss quadrature rule the normal flux is computed at different locations in the element face. At each quadrature point we consider a one-dimensional Riemann problem and neglect the tangential variation of the solution in the element face. The tangential vectors at the quadrature points are slightly different and this results in different shear wave contributions from the quadrature points, which manifest themselves in spurious entropy generation near the wall. The Taylor quadrature rule considers the Riemann problem only at one point and therefore results in a more consistent discretization when combined with one-dimensional (approximate) Riemann solvers.

The use of quadratic superparametric elements in combination with the Taylor quadrature rule further reduces the maximum total pressure loss to 0.018, see Figures 3 and 4. Incorporating the boundary curvature effects in combination with the Taylor quadrature rule also results in a significantly improved solution, see Figure 5 which shows the Mach number contours. The contours are now nearly symmetric with respect to $x = 0$ and do not show the pronounced wake visible in Figure 2.
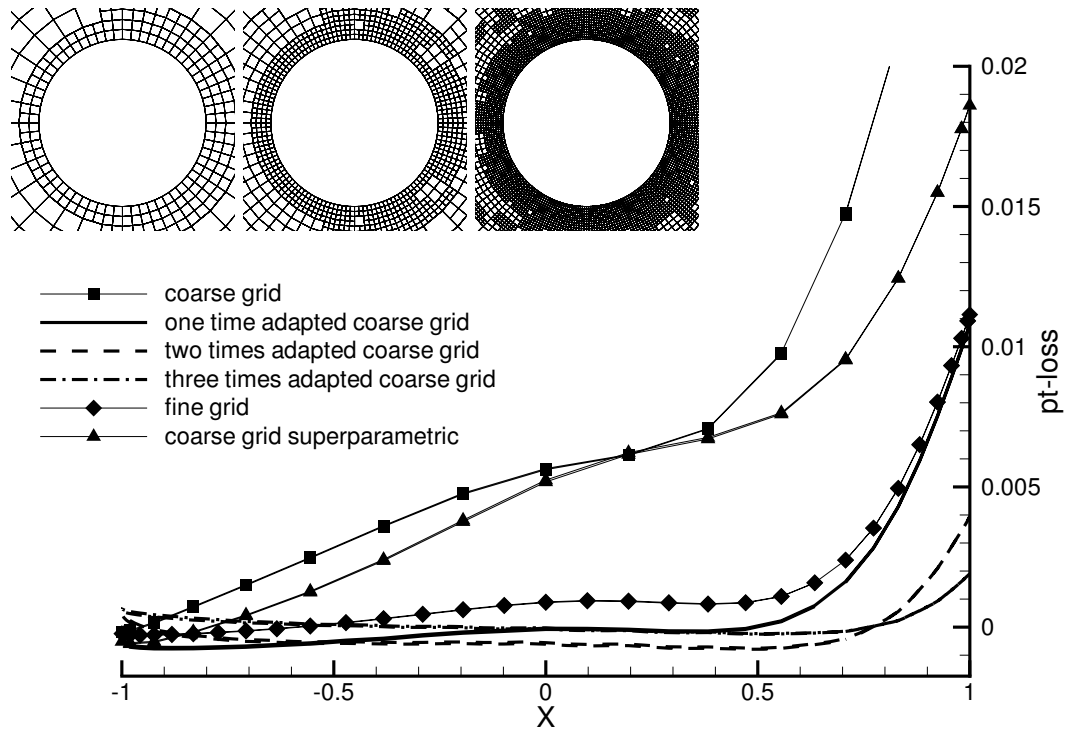
Fig. 6   Comparison of the total pressure at the wall of a circular cylinder at $M_\infty = 0.38$ using Taylor quadrature with locally refined linear isoparametric elements (meshes 1536, 1710, 2439, 8358 elements, pressure from Riemann problem).

Local mesh adaptation in the vicinity of the wall can also be a very efficient technique to reduce the numerical error at slip flow boundaries. Especially, when it is related to the boundary curvature as discussed in Section 7. Figure 6 shows three meshes obtained with local refinement of a 32×48 mesh with linear isoparametric elements. The flux quadrature is done with the Taylor quadrature rule. The adapted meshes contain 1536, 1710, 2439, 8358 elements. Refinement is based on the generated vorticity, which should be zero in this subsonic inviscid flow. Also shown is the total pressure loss on the adapted mesh, on the coarse mesh with isoparametric and superparametric elements, and on the fine mesh with 64×96 elements. Figure 6 shows that after three adaptations the total pressure loss is nearly reduced to zero, except close to the rear stagnation point. The fine grid result is nearly identical to the one-time adapted mesh but requires 3.6 times more elements than the one-time adapted mesh. The Mach number contours on the fine mesh are shown in Figure 7 and are nearly symmetric with respect to the axis $x = 0$.
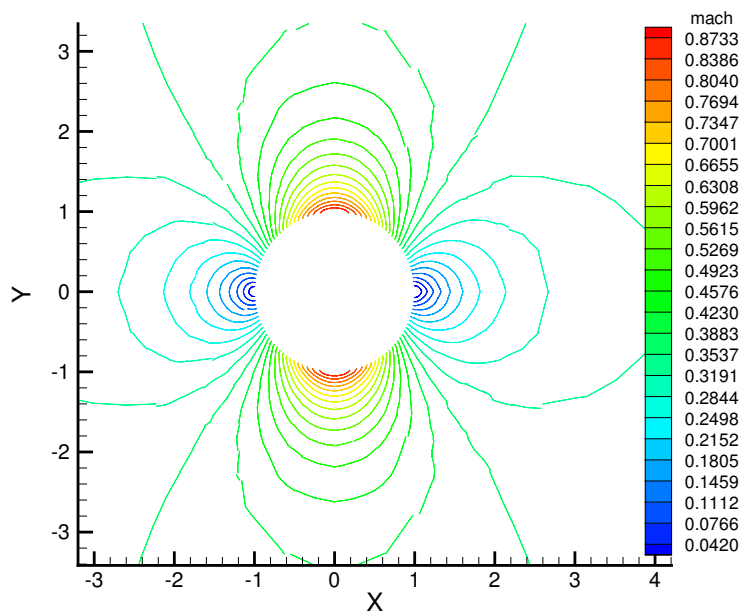
Fig. 7   Mach contours for flow about a circular cylinder at $M_\infty = 0.38$ using Taylor quadrature on a locally refined mesh with 8358 linear isoparametric elements, pressure from Riemann problem.

9 Conclusions

Discontinuous Galerkin finite element discretizations of the Euler equations of gas dynamics can suffer from significant numerical errors due to slip flow boundary conditions at curved walls, depending on the type of numerical quadrature and the representation of the domain boundary. The newly presented Taylor flux quadrature rule results in a significant reduction of the total pressure losses in comparison with a two-point (product) Gauss quadrature rule. A simple analysis has shown that for a consistent boundary discretization in a discontinuous Galerkin finite element method it is necessary to take the effect of the domain boundary curvature into account. This is demonstrated with quadratic superparametric elements, which reduces the total pressure losses both for Gauss and Taylor quadrature rules. Superparametric elements are the most effective for Taylor quadrature rules where they result in more than a factor three reduction in total pressure loss in comparison with isoparametric elements combined with Gauss quadrature. The effects of boundary curvature can also be removed using mesh adaptation and it is demonstrated that it is not necessary to use a higher-order boundary representation as was stated by Bassi and Rebay (Ref. 1). Local mesh refinement of linear isoparametric elements is very effective in reducing the error at slip flow boundaries and can provide an alternative to the use of superparametric elements.

References

1. F. Bassi and S. Rebay, High-order accurate discontinuous finite element solution of the 2D Euler equations, *J. Comput. Phys.*, **138**, 251-285 (1997).

2. P. Batten, N. Clarke, C. Lambert and D. Causon, On the choice of wave speeds for the HLLC Riemann solver, *SIAM J. Sci. and Stat. Comp.*, **18**, 1553-1570 (1997).

3. C.E. Baumann and T.J. Oden, A discontinuous hp finite element method for the Euler and the Navier-Stokes equations, *Int. J. Numer. Meth. Fluids*, **47**, 61-73 (2000).

4. B. Cockburn, Devising discontinuous Galerkin methods for non-linear hyperbolic conservation laws, *J. Comput. Appl. Math.*, **128**, 187-204 (2001).

5. B. Cockburn and C.W. Shu, Runge-Kutta Discontinuous Galerkin Methods for convection-dominated problems, *J. Sci. Comput.*, **16**, 173-261 (2001).

6. E.F. Toro, M. Spruce and W. Speares, Restoration of the contact surface in the HLL-Riemann solver, *Shock Waves*, **4**, 25-34 (1994).

7. E.F. Toro, *Riemann solvers and numerical methods for fluid dynamics. A practical introduction* 2nd edition (Springer Verlag, 1999).

8. J.J.W. van der Vegt and H. van der Ven, Discontinuous Galerkin finite element method with anisotropic local grid refinement for inviscid compressible flows, *J. Comput. Phys.* **141**, 46-77 (1998).

9. J.J.W. van der Vegt and H. van der Ven, Space-time discontinuous Galerkin finite element method with dynamic grid motion for inviscid compressible flows. I. General formulation, to appear *J. of Comput. Phys.* (2002).

10. H. van der Ven and J.J.W. van der Vegt, Space-time discontinuous Galerkin finite element method with dynamic grid motion for inviscid compressible flows. II. Efficient flux quadrature, to appear *Comput. Meth. Appl. Mech. Engrg.* (2002).